Journal of Materials Chemistry A

COMMUNICATION

View Article Online
View Journal | View Issue

Cite this: J. Mater. Chem. A, 2015, 3, 9146

Received 2nd March 2015
Accepted 24th March 2015

DOI: 10.1039/c5ta01595b

www.rsc.org/MaterialsA

Organic solvent vapor sensitive methylammonium lead trihalide film formation for efficient hybrid perovskite solar cells

Jiarong Lian,[ab] Qi Wang,[a] Yongbo Yuan,[a] Yuchuan Shao[a] and Jinsong Huang*[a]

The anisotropic electronic properties of the perovskite crystals originating from their non-cubic crystal structures can potentially give rise to the grain orientation correlated photovoltaic device performance. Here we report that an organic solvent vapor atmosphere introduced during the spin-coating and formation of perovskite films changes the orientation and size of perovskite grains. It was found that slightly larger but much more oriented methylammonium lead trihalide ($CH_3NH_3PbI_3$) grains could be obtained under 1,2-dichlorobenzene (DCB) and dimethyl sulfoxide (DMSO) vapor atmospheres. The devices with more oriented grains outperformed regular devices with more random grains by a 50 mV larger open circuit voltage as well as a slightly increased fill factor. The device efficiency enhancement can be attributed to the longer charge recombination lifetime resulting from the reduced trap density and oriented grains. This result is important in providing guidelines for comparing the results from various groups because organic solvent vapors are generally present in a sealed glovebox for perovskite solar cell fabrication.

A class of compounds named organometal trihalide perovskites (OTPs) that were first uncovered in the Ural Mountains more than a century ago, right now a rock star in the field of solar-energy research, exhibit numerous appealing features, including very strong light absorption, large bipolar carrier mobility, free charge generation under illumination, and long exciton diffusion lengths.[1–3] OTP devices have shown an unprecedented increase in power conversion efficiency (PCE) from 3.8% in 2009 (ref. 4) to around 10% in 2012 (ref. 5) and a certified efficiency of 20.1% in early 2015.[6] By analyzing the attainable photocurrent and photovoltage, increasing the PCE of perovskite solar cells to 30% is also realistic with a tandem structure with well-established c-Si solar cells.[7] Therefore, their high efficiencies and low-cost solution process make perovskite solar cells an extremely commercially attractive option.[8]

The quality of perovskite films, such as morphology and crystallinity, has been shown to strongly influence the overall photovoltaic performance of devices.[1,9] The preferred hybrid perovskite films to date fulfill several criteria, high film uniformity, complete film coverage without pin-holes, and large perovskite crystallite grains, to harness their excellent carrier transport properties.[9,10] Many efforts have been devoted to improving the film morphology and coverage *via* optimizing the fabrication protocols during the film formation process, including the change of precursor composition,[5,11] solvent engineering,[12,13] optimizing the deposition & annealing temperature, *etc.*[14,15] We have reported a simple method to form the most continuous, compact iodine perovskite ($CH_3NH_3PbI_3$, $MAPbI_3$) films by the interdiffusion of spin-coated stacking layers of PbI_2 and MAI assisted by thermal annealing.[16] To increase the perovskite crystallinity and grain size, some additives are incorporated to facilitate homogenous nucleation and modulate the kinetics of growth during crystallization,[1] and a solvent annealing method has also been developed by us.[10]

In our previous study of using solvent-annealing to enhance the grain size of the polycrystalline film, organic solvent vapors were introduced during the thermal annealing process of perovskite layers. Since the solid perovskite films already formed after 90 second thermal annealing, the solvent vapors in the solvent annealing were expected to facilitate the grain growth and grain coalescence by providing a higher ion diffusion mobility environment. In this study, we introduce the solvent vapor during the perovskite formation stage which is the spin-coating of MAI on PbI_2. According to the formation process of the perovskite film by the two-step interdiffusion method, perovskite nucleation is expected to occur first at the MAI/PbI_2 interface.[16] It was found that both larger and oriented grains could be obtained for the $MAPbI_3$ film by introducing 1,2-dichlorobenzene (DCB) and dimethyl sulfoxide (DMSO) atmospheres. DMSO and DCB were chosen because they are the frequently used solvents in device fabrication and vapors of

[a]Department of Mechanical and Materials Engineering, Nebraska Center for Materials and Nanoscience, University of Nebraska–Lincoln, Lincoln, Nebraska 68588-0656, USA. E-mail: jhuang2@unl.edu

[b]Key Laboratory of Optoelectronic Devices and Systems of Ministry of Education and Guangdong Province, College of Optoelectronic Engineering, Shenzhen University, Shenzhen, China, 518060

these solvents are always present in gloveboxes. Therefore understanding the influence of these solvent vapors on the film morphology and device performance provides insight into the comparison of the device performance in many laboratories.

The solvent vapor modulated spin-coating process of the PbI_2/MAI stacking layer is illustrated in Fig. 1. For the film fabrication, PbI_2 and MAI were first dissolved in dimethylformamide (DMF) and isopropanol (IPA) with a concentration of 400 mg ml^{-1} and 40 mg ml^{-1}, respectively. Poly(3,4-ethylenedioxythiophene)poly(styrenesulfonate) (PEDOT:PSS) was spin coated on a pre-cleaned indium tin oxide (ITO) glass substrate at a spin-rate of 3000 rpm for 60 seconds. 25 nm thick PEDOT:PSS films were annealed at 135 °C for 20 minutes. Hot PbI_2 precursor solution (70 °C) was spin-coated on the PEDOT:PSS surface at a spin-rate of 6000 rpm for 35 seconds in a nitrogen filled glove-box, then the PbI_2 films were dried at 70 °C for 15 minutes. Here the DCB and DMSO solvent vapors were generated by heating the solvent-filled flask (150 μl DCB or DMSO in a 50 ml size flask) at 100 °C, and the evaporated solvent vapor was guided *via* a tube onto the top of the PbI_2 films. It is noted that the DMSO additive[12] was used to engineer the kinetics of grain growth. The difference here is DMSO or DCB was introduced in the vapor phase, which explains the influence of the vapor environment on the device fabrication. After the PbI_2 films were soaked in different vapor atmosphere for about 15 seconds, the MAI solution was spin-coated on the top of PbI_2 films at a spin-rate of 6000 rpm for 35 seconds. The spin-coated MAI layers were dried at 70 °C for 10 minutes, and further annealed at 100 °C for 60 minutes. In order to passivate the surface defects of the perovskite films, 20 nm thickness phenyl-C61-butyric acid methyl ester (PCBM) films were coated on the perovskite layers. After that, 20 nm C_{60}, 7 nm 2,9-dimethyl-4,7-diphenyl-1,10-phenanthroline (BCP) and 100 nm aluminum layers were sequentially deposited by thermal evaporation. The resulting devices have a structure of ITO/PEDOT:PSS (25 nm)/$MAPbI_3$ (280 nm)/PCBM (20 nm)/C_{60} (20 nm)/BCP (8 nm)/Al (100 nm).

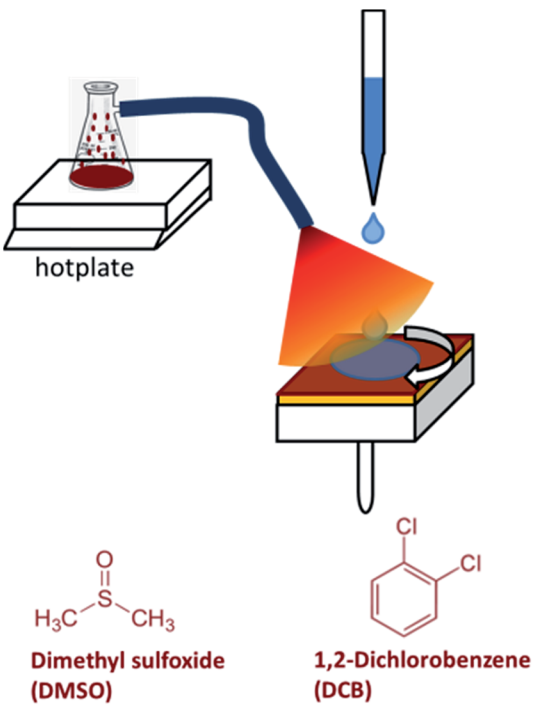

Fig. 1 Schematic illustration of the solvent spin-coating process where the solvent vapor was generated by heating DMSO and DCB solvents and the vapor was directed by a tube to the film surface during the spin-coating process. The chemical structures of DMSO and DCB solvents are also shown.

The influence of the organic solvent vapor treatment during the film formation process on the morphology and microstructure of the $MAPbI_3$ films was examined by scanning electron microscopy (SEM) and X-ray diffraction (XRD). As shown in Fig. 2, DCB and DMSO vapor treated $MAPbI_3$ films show slightly larger grains than those of the control $MAPbI_3$ film formed under a N_2 atmosphere with the average grain size increased from 180 nm to 230 nm and 300 nm, respectively. The XRD measurement results shown in Fig. 3 also show a stronger diffraction peak intensity for the DCB and DMSO vapor treated $MAPbI_3$ films, which indicates better crystallinity of the solvent vapor treated $MAPbI_3$ films. The mean coherent scattering domain size calculated from the half width of the XRD peaks according to the Debye–Scherrer formula increased from 60 nm for the N_2 treated $MAPbI_3$ film to 68 nm for the DCB vapor treated $MAPbI_3$ film, and to 76 nm for the DMSO vapor treated $MAPbI_3$ film.

By taking a closer look at the XRD spectra, one may find that the relative intensity for each peak has changed, which indicates the grain orientation changes for these $MAPbI_3$ films. To illustrate the degree of grain orientation variation of the $MAPbI_3$ polycrystalline grains, we normalized the XRD peaks to the peak at 14.17°, *i.e.* the (110) plane, and plotted the spectra against the azimuth angle ω in Fig. 3b. It is obvious that all the other XRD peaks for the planes except the (110) plane, including (112), (202), (312), (224), and (314), have much lower intensity, which suggests increased (110) orientation of the polycrystalline $MAPbI_3$ films, and the long axis preferentially stayed parallel to the substrate for DCB and DMSO treated $MAPbI_3$ films. Here it should be noted that regular thermal annealing and solvent-annealing treatments do not cause the grain orientation change despite the increasing grain size,[10,17,18] which is absolutely different from our case using the solvent spin coating method.

Because of the large size of the iodine atoms, the $MAPbI_3$ crystal should be tetragonal or orthorhombic with a distorted PbI_6^{4-} octahedral structure.[19] It is thus natural to hypothesize that $MAPbI_3$ crystals have anisotropic electronic properties. It is interesting to note that nearly all the high performance perovskite solar cells have the long axis of the $MAPbI_3$ films preferentially oriented parallel to the substrate, where the planes of (110), (220), and (330) exhibit the strongest intensity in the X-ray diffraction (XRD) spectra.[5,9,10] In addition, some other studies found that increasing immersion solution temperatures can realize the preferential orientation of the (110) plane without changing the crystal size, and the corresponding devices achieve higher short circuit currents.[20] Saliba *et al.* also fabricated high performance devices with larger crystal sizes and more

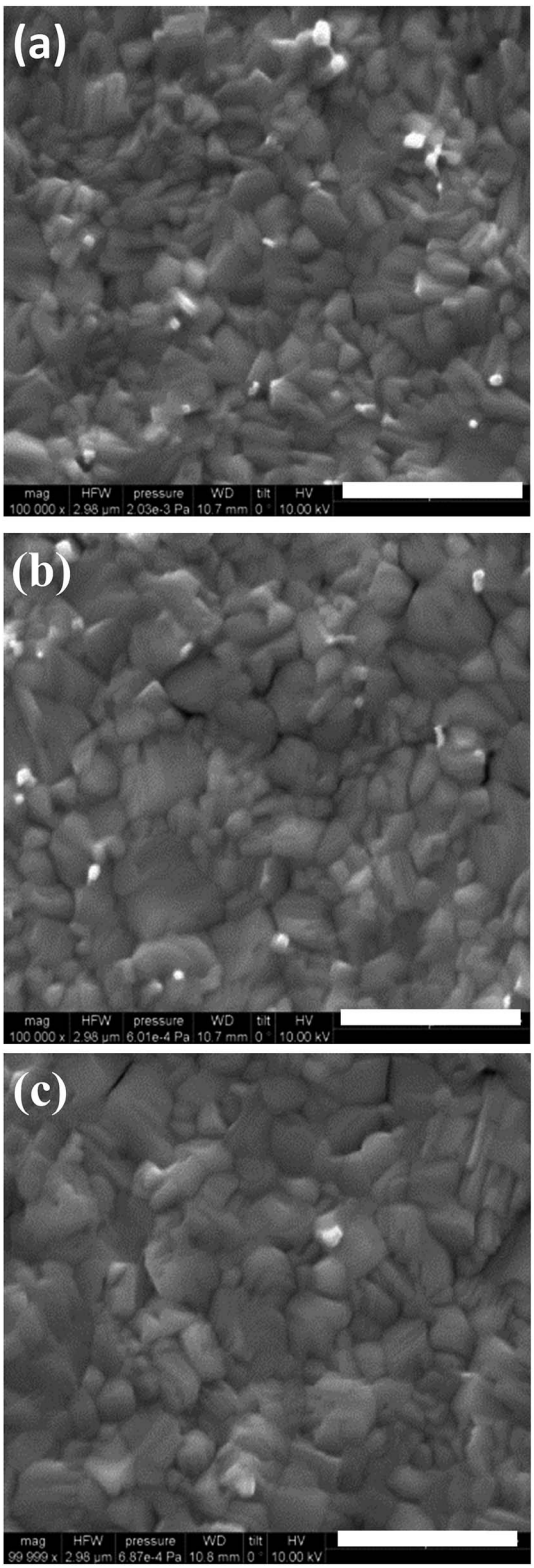

Fig. 2 The surface topography measured by SEM for different perovskite films fabricated in the atmosphere of (a) N_2, (b) DCB vapor, and (c) DMSO vapor, respectively. The scale bar is 1 μm.

oriented domains *via* a flash annealing procedure, in which the samples were first held at 100 °C for 5 min, then rapidly heated to 130 °C in <3 min, and held there for another 5 min.[14] These

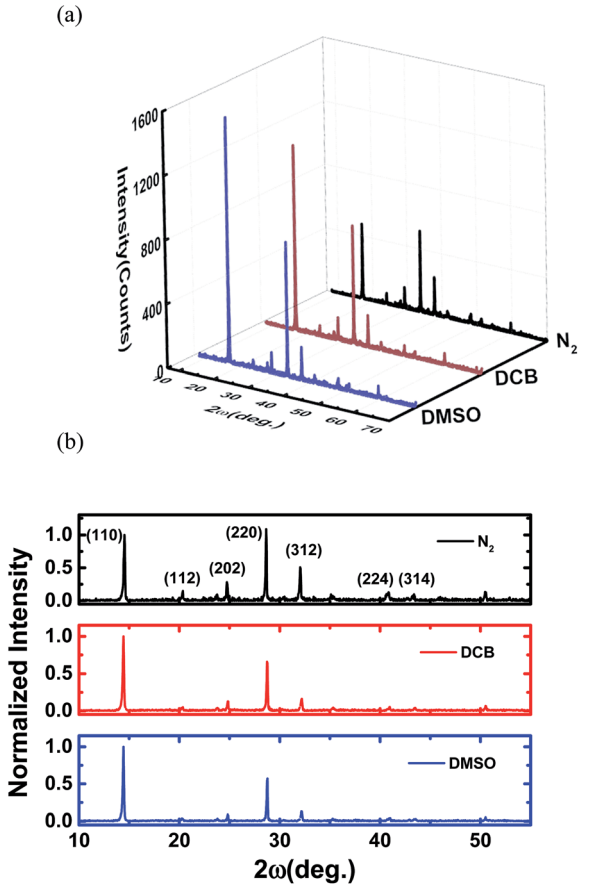

Fig. 3 (a) The absolute and (b) normalized intensity X-ray diffraction spectra of perovskite samples fabricated in N_2, DCB, and DMSO conditions, respectively.

studies suggest that controlling the deposition parameters to achieve highly oriented crystalline domains can be a new route to enhance the efficiency of perovskite solar cells.

Photovoltaic devices were fabricated to evaluate the influence of enlarged grain size and increased (110) orientation on the device performance. Fig. 4 shows the photocurrent density (J) at different bias for the devices, and the performance of the devices is summarized in Table 1. DCB and DMSO treatments barely changed the short current density (J_{sc}), but obviously

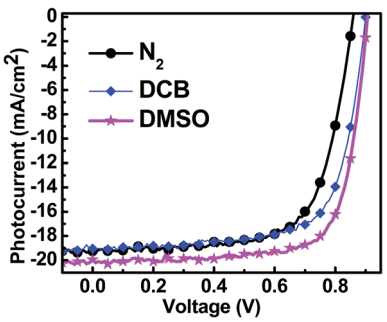

Fig. 4 Photocurrent (J) *versus* voltage (V) curves for solar cells fabricated under atmosphere of N_2 and DCB, and DMSO vapors, respectively.

increased the open-circuit voltage (V_{oc}) from 0.85 V to 0.90 V, and also enlarged the fill factor (FF) from 65.8% to more than 70%. The PCE is increased from 11.4% to 12.1% and 13.6% for the DCB and DMSO treated devices, respectively. It is noted that these devices do not have the highest efficiency because of the different fabrication methods used, for example, solvent annealing was not applied in this study. All the three devices had the same series resistance (R_s) value of 70 ohm cm^{-2}, but exhibit obviously different shunt resistance (R_{sh}) values. R_{sh} is an indication of the amount of current leakage paths in a solar cell device, which is caused by the crystal defects or impurities. Therefore the DMSO treated perovskite films, which show the largest R_{sh} of all three devices, should have the lowest concentration in crystal defects or impurities. This is consistent with the SEM and XRD measurement results. The largest grains in DMSO treated perovskite films provide the lowest grain boundary area, and more oriented grains result in less large angle grain boundaries which can be highly leakage paths. The incident-photon-to-current conversion efficiency (IPCE) spectra of all the devices are similar, which is in good agreement with their comparable J_{sc}. Since the photocurrent hysteresis could cause inaccurate characterization of the device efficiency, we further measured J–V curves with different scanning rates in the range of 0.02 V s^{-1} to 0.5 V s^{-1} and changed scanning directions with a scanning rate of 0.1 V s^{-1}. All the devices showed nearly the same J–V curves without obvious photocurrent hysteresis observed. This can be explained by the sophisticated passivation techniques we applied using a double layer fullerene.[21]

The increase of device V_{oc} and FF can be explained by the reduction of trap density of DMSO and DCB treated perovskite films. The V_{oc} for the given photoactive materials is determined by the equation:[22]

$$V_{oc} = \frac{k_B T}{q} \ln\left(\frac{J_{sc}}{J_o}\right) \quad (1)$$

where k_B, T, q, J_{sc}, and J_o stand for the Boltzmann constant, absolute temperature, electron charge, short current density, and saturated reversed current density, respectively. A larger R_{sh} is expected to give a lower saturated reversed current density and thus enhance the device V_{oc}. The reduction of J_o can be correlated with the fewer defects and longer carrier lifetime since J_o is governed by

$$J_o = \frac{qW N_c^{1/2} N_v^{1/2}}{\sqrt{\tau_p \tau_n}} \exp\left[-\frac{E_g}{k_B T}\right] \quad (2)$$

where W, $N_{c(v)}$, and $\tau_{p(n)}$ are the total depletion width, effective conduction (valence) band density of states, and lifetime of minority holes (electrons), respectively.

To verify the lower charge trap density and longer carrier lifetime in the DMSO and DCB treated perovskite films, we used thermal admittance spectroscopy (TAS) and impedance spectroscopy to directly measure the trap density of states (tDOS) and charge recombination lifetime under device working conditions, *i.e.*, under 1 sun illumination. TAS is an established and effective technique to measure the trap density in thin-film solar cells.[23] Experimental details and calculations of the tDOS can be found elsewhere.[10] As shown in Fig. 5a, the tDOS of the devices with DMSO treated perovskite films are obviously smaller than those treated in N_2 or DCB vapor. The total trap density, calculated by integrating the tDOS into a trap depth of 0.33 eV to 0.41 eV, for the DMSO treated device is 7.0 $\times$ 10^{15} m^{-3}, which is three-times smaller than that of the N_2 treated device (2.1 $\times$ 10^{16} m^{-3}). Therefore it is natural to correlate the reduced trap density with the enhanced device V_{oc} and FF because a lower trap density gives rise to a reduced charge recombination, which boosts V_{oc} and FF. Again the reduced trap density can be explained by the larger and oriented grains in DMSO treated perovskite films because the grain boundaries are rich in defects based on our previous experimental and theoretical study.[21] The carrier recombination lifetime result, as shown in Fig. 5b, is consistent with the trap density measurement results. The lower trap density in a DMSO treated perovskite film gives a longer carrier recombination lifetime.

In summary, we have investigated the influence of solvent vapor introduced during the spin-coating process on the film morphology and the associated device performance. It was found that slightly larger grain size and obviously preferred orientation of the (110) plane for $MAPbI_3$ films were obtained for DCB and DMSO treated films, which contributed to the observed reduced trap density and longer carrier lifetime in these films. The photovoltaic performance of the devices with DCB and DMSO treated films also showed increased V_{oc} and FF, which can be explained by the lower trap density in these films. This study reveals the sensitivity of the perovskite film to the atmosphere during the formation of perovskite films, which is particularly important for comparing and interpreting the results from different research groups.

Table 1 The performance metrics extracted from J–V measurements under standard AM1.5G illumination (100 mW cm^{-2}) for the best device performance and average performance using different spin coating atmospheres

Vapor atmosphere		J_{sc} (mA cm^{-2})	V_{oc} (V)	PCE (%)	FF (%)	R_s (ohm cm^{-2})	R_{sh} (ohm cm^{-2})
N_2	Best	19.25	0.86	11.35	68.5	70	1425
	Average	19.32	0.85	10.80	65.7		
DCB	Best	19.04	0.90	12.13	70.6	70	3071
	Average	19.02	0.90	12.09	70.6		
DMSO	Best	20.00	0.90	13.60	75.1	70	4986
	Average	19.90	0.89	12.84	72.5		

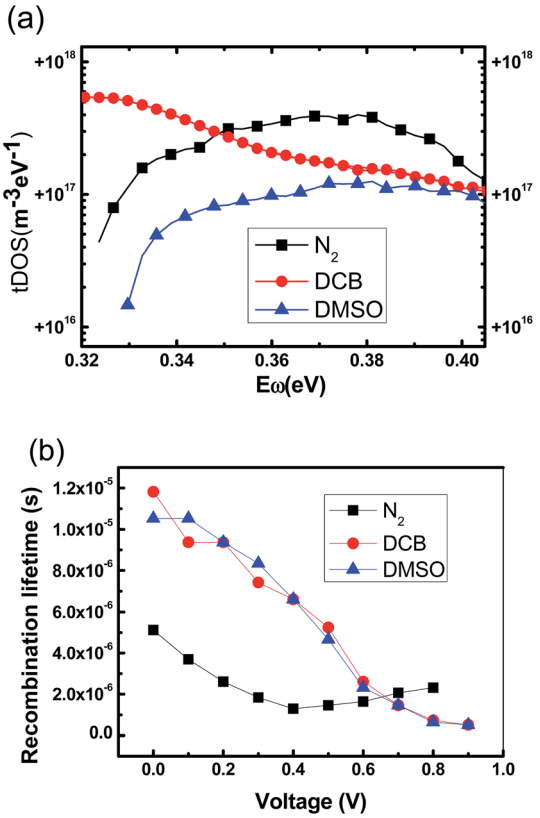

Fig. 5 (a) Trap-density of states measured from the thermal admittance spectroscopy measurements, and (b) carrier recombination lifetime of the devices with perovskite films treated by N_2, and DCB, and DMSO vapors.

Acknowledgements

We thank the financial support from the Department of Energy under Award DE-EE0006709 and the Nebraska Public Power District through the Nebraska Center for Energy Sciences Research.

References

1 P.-W. Liang, C.-Y. Liao, C.-C. Chueh, F. Zuo, S. T. Williams, X.-K. Xin, *et al.* Additive Enhanced Crystallization of Solution-Processed Perovskite for Highly Efficient Planar-Heterojunction Solar Cells, *Adv. Mater.*, 2014, **26**, 3748–3754.

2 R. F. Service, Perovskite Solar Cells Keep On Surging, *Science*, 2014, **344**, 458.

3 M. D. McGehee, Perovskite solar cells: Continuing to soar, *Nat. Mater.*, 2014, **13**, 845–846.

4 A. Kojima, K. Teshima, Y. Shirai and T. Miyasaka, Organometal halide perovskites as visible-light sensitizers for photovoltaic cells, *J. Am. Chem. Soc.*, 2009, **131**, 6050–6051.

5 M. M. Lee, J. Teuscher, T. Miyasaka, T. N. Murakami and H. J. Snaith, Efficient Hybrid Solar Cells Based on Meso-Superstructured Organometal Halide Perovskites, *Science*, 2012, **338**, 643–647.

6 http://www.nrel.gov/ncpv/images/efficiency_chart.jpg, the National Renewable Energy Laboratory.

7 P. Gao, M. Gratzel and M. K. Nazeeruddin, Organohalide lead perovskites for photovoltaic applications, *Energy Environ. Sci.*, 2014, **7**, 2448–2463.

8 http://www.wsj.com/articles/perovskite-offers-shot-at-cheaper-solar-energy-1411937799, Perovskite Offers Shot at Cheaper Solar Energy, The Wall Street Journal.

9 M. Liu, M. B. Johnston and H. J. Snaith, Efficient planar heterojunction perovskite solar cells by vapour deposition, *Nature*, 2013, **501**, 395–398.

10 Z. Xiao, Q. Dong, C. Bi, Y. Shao, Y. Yuan and J. Huang, Solvent Annealing of Perovskite-Induced Crystal Growth for Photovoltaic-Device Efficiency Enhancement, *Adv. Mater.*, 2014, **26**, 6503–6509.

11 A. Abrusci, S. D. Stranks, P. Docampo, H.-L. Yip, A. K. Y. Jen and H. J. Snaith, High-Performance Perovskite–Polymer Hybrid Solar Cells *via* Electronic Coupling with Fullerene Monolayers, *Nano Lett.*, 2013, **13**, 3124–3128.

12 H.-B. Kim, H. Choi, J. Jeong, S. Kim, B. Walker, S. Song, *et al.* Mixed solvents for the optimization of morphology in solution-processed, inverted-type perovskite/fullerene hybrid solar cells, *Nanoscale*, 2014, **6**, 6679–6683.

13 C.-C. Chueh, C.-Y. Liao, F. Zuo, S. T. Williams, P.-W. Liang and A. K. Y. Jen, The roles of alkyl halide additives in enhancing perovskite solar cell performance, *J. Mater. Chem. A*, 2015, DOI: 10.1039/c4ta05012f.

14 M. Saliba, K. W. Tan, H. Sai, D. T. Moore, T. Scott, W. Zhang, *et al.* Influence of Thermal Processing Protocol upon the Crystallization and Photovoltaic Performance of Organic–Inorganic Lead Trihalide Perovskites, *J. Phys. Chem. C*, 2014, **118**, 17171–17177.

15 A. Dualeh, N. Tétreault, T. Moehl, P. Gao, M. K. Nazeeruddin and M. Grätzel, Effect of Annealing Temperature on Film Morphology of Organic–Inorganic Hybrid Pervoskite Solid-State Solar Cells, *Adv. Funct. Mater.*, 2014, **24**, 3250–3258.

16 Z. Xiao, C. Bi, Y. Shao, Q. Dong, Q. Wang, Y. Yuan, *et al.* Efficient, high yield perovskite photovoltaic devices grown by interdiffusion of solution-processed precursor stacking layers, *Energy Environ. Sci.*, 2014, **7**, 2619–2623.

17 C. Bi, Y. Shao, Y. Yuan, Z. Xiao, C. Wang, Y. Gao, *et al.* Understanding the formation and evolution of interdiffusion grown organolead halide perovskite thin films by thermal annealing, *J. Mater. Chem. A*, 2014, **2**, 18508–18514.

18 K. W. Tan, D. T. Moore, M. Saliba, H. Sai, L. A. Estroff, T. Hanrath, *et al.* Thermally Induced Structural Evolution and Performance of Mesoporous Block Copolymer-Directed Alumina Perovskite Solar Cells, *ACS Nano*, 2014, **8**, 4730–4739.

19 J. A. McLeod, Z. Wu, P. Shen, B. Sun and L. Liu, Self-Alignment of the Methylammonium Cations in Thin-Film Organometal Perovskites, *J. Phys. Chem. Lett.*, 2014, **5**, 2863–2867.

20 P. Docampo, F. C. Hanusch, N. Giesbrecht, P. Angloher, A. Ivanova and T. Bein, Influence of the orientation of

methylammonium lead iodide perovskite crystals on solar cell performance, *APL Mater.*, 2014, **2**, 081508.
21 Y. Shao, Z. Xiao, C. Bi, Y. Yuan and J. Huang, Origin and elimination of photocurrent hysteresis by fullerene passivation in CH3NH3PbI3 planar heterojunction solar cells, *Nat. Commun.*, 2014, **5**, 5784.
22 S. C. Singh, *Solar Photovoltaics: Fundamentals, Technologies and Applications*, PHI Learning Pvt. Ltd., 2011.
23 J. Heath and P. Zabierowski, Capacitance Spectroscopy of Thin-Film Solar Cells, *Advanced Characterization Techniques for Thin Film Solar Cells*, Wiley-VCH Verlag GmbH & Co. KGaA, 2011, pp. 81–105.